Reprinted from:
LASER INTERACTIONS AND
RELATED PLASMA PHENOMENA, Vol. 3
(Plenum Press, 1974)

PHYSICAL MECHANISMS FOR LASER-PLASMA PARAMETRIC INSTABILITIES*

Francis F. Chen†

University of California, Los Angeles

Los Angeles, California 90024

During the past year, there has been a profusion of theoretical results concerning parametric instabilities, anomalous backscattering, and other nonlinear interactions expected to occur at the large laser intensities needed to achieve fusion. It is often difficult for the experimentalist to gain an intuitive grasp of the important physical mechanisms involved. Fortunately, most of these phenomena are generalized parametric instabilities which can be explained, both qualitatively and quantitatively, by simple physical descriptions involving the ponderomotive force.

THE PONDEROMOTIVE FORCE

Originally invoked[1] in connection with laser interactions to explain fast-ion production, the ponderomotive force is nothing more than radiation pressure in a plasma. It is most readily understood from the single-particle point of view. Following Schmidt[2], we write the equation of motion for a single electron moving in a wave:

$$m \frac{d\underline{v}}{dt} = -e[\underline{E}(\underline{r}) + \frac{1}{c} \underline{v}\times\underline{B}(\underline{r})] \quad , \tag{1}$$

*Presented at the Third Workshop on "Laser Interaction and Related Plasma Phenomena" held at Rensselaer Polytechnic Institute, Troy, New York, August 13-17, 1973.

†This work was supported by the U.S. Atomic Energy Commision, Contract AT(04-3)-34, Project 157, Mod. 6, Task II.

where

$$\underline{E}(\underline{r}) = \underline{E}_s(\underline{r})\cos\omega_0 t \tag{2}$$

and

$$\underline{B}(\underline{r}) = -\frac{c}{\omega_0}\,\underline{\nabla}\times\underline{E}_s \sin\omega_0 t \quad \text{(Maxwell's equation)} \; . \tag{3}$$

The $\underline{v}\times\underline{B}$ term in Eq. (1) is v_0/c times smaller than the $\underline{E}$ term (v_0 will be defined below), and to lowest order the electron oscillates in the direction of $\underline{E}$:

$$\underline{v}^{(1)} = -\frac{e}{m\omega_0}\,\underline{E}_s \sin\omega_0 t \quad . \tag{4}$$

We define the quiver velocity v_0 to be the peak value of $v^{(1)}$ in a plane-polarized wave ($E_0 = |E_s\max|$):

$$v_0 \equiv \frac{eE_0}{m\omega_0} \tag{5}$$

When the quantity v_0/c, which characterizes the strength of nonlinear interactions, is small but finite, we can use $\underline{v}^{(1)}$ to solve Eq. (1) to the next order. We must also expand $\underline{E}(r)$ about the initial position $\underline{r}_0$, for Eq. (1) holds in the frame moving with the electron. Thus

$$\underline{E}(\underline{r}) \approx E(r_0) + \delta\underline{r}\cdot\underline{\nabla}\,\underline{E} \quad , \tag{6}$$

where $\delta\underline{r}$ is given by the integral of Eq. (4):

$$\delta\underline{r} = \frac{e}{m\omega_0^2}\,\underline{E}_s\cos\omega_0 t \quad . \tag{7}$$

Thus

$$m\,\frac{d\underline{v}^{(2)}}{dt} = -e[\delta\underline{r}\cdot\underline{\nabla}\,\underline{E}(\underline{r}_0) + \frac{1}{c}\,\underline{v}^{(1)}\times\underline{B}(\underline{r}_0)] \; . \tag{8}$$

Using Eqs. (7), (4), and (3) and averaging over time, we find the secular force acting on the electron:

$$\underline{f}_{NL} \equiv m < \frac{d\underline{v}^{(2)}}{dt} > = -\frac{e^2}{m\omega_0^2}\,\frac{1}{2}\,(\underline{E}_s\cdot\underline{\nabla}\,\underline{E}_s + \underline{E}_s\times\underline{\nabla}\times\underline{E}_s) \quad . \tag{9}$$

The $\underline{E}\times\underline{\nabla}\times\underline{E}$ term gives rise to a drift of the electrons in the direction of the wave. This is caused by the wave magnetic field, which distorts the linear orbit of the electron into a figure-8 path, as described by Hora[1]. This term drives the backscattering instabilities. The $\underline{E}\cdot\underline{\nabla}\,\underline{E}$ term is due to the finite excursion of the oscillating electron, which brings it into regions of different field intensity. This term is equivalent to the $\underline{v}\cdot\underline{\nabla}\,\underline{v}$ convection

term in the fluid equation. The electrostatic parametric instabilities are driven by this term.

The ponderomotive force F_{NL} is the force per unit volume, $n_e \underline{f}_{NL}$:

$$\underline{F}_{NL} = -\frac{\omega_p^2}{\omega_0^2} \underline{\nabla} \left(\frac{E_s^2}{16\pi} \right) = -\frac{\omega_p^2}{\omega_0^2} \underline{\nabla} \frac{\langle E^2 \rangle}{8\pi} \quad , \tag{10}$$

where $\omega_p^2 = 4\pi n_e e^2/m$, and the average is over a wavelength.

Although the corresponding force on the ions is m/M times smaller, the force $\underline{F}_{NL}$ on the electrons is transmitted to the ions by self-consistent fields, provided (a) there are density gradients, and (b) $\underline{F}_{NL}$ varies in time more slowly than the ion plasma frequency ω_{pi}. As the electrons respond to $\underline{F}_{NL}$, they generate a charge-separation electric field $\underline{E}_1$ such that $\underline{F}_{NL} - n_e e \underline{E}_1 = 0$. The ions feel a force $n_i e \underline{E}_1$, and the total force density in the quasineutral plasma is therefore $\underline{F}_{NL}$.

Eq. (10) can also be derived[3] from the macroscopic viewpoint, considering the plasma to be a dielectric with $\varepsilon = 1-\omega_p^2/\omega^2$, but the physics is then more obscure. One can consider $\underline{F}_{NL}$ to be a radiation pressure

$$\underline{F}_{NL} = -\underline{\nabla} \frac{\langle E^2 \rangle}{8\pi} - \underline{\nabla} \frac{\langle B^2 \rangle}{8\pi} \quad , \tag{11}$$

but this expression does not contain the plasma density explicitly. To see how the density enters, consider first the case of a vacuum. If the wave were infinite, the field strength would be uniform, and $\underline{F}_{NL}$ would be zero. If the wave were reflected from a perfect mirror, $\underline{F}_{NL}$ would still vanish, because there is no preferred direction for it. Fig. 1 shows that in the standing wave pattern $\nabla\langle E^2\rangle/8\pi$ is always equal and opposite to $\nabla\langle B^2\rangle/8\pi$. On the other hand, if the wave were reflected from the cutoff layer of an

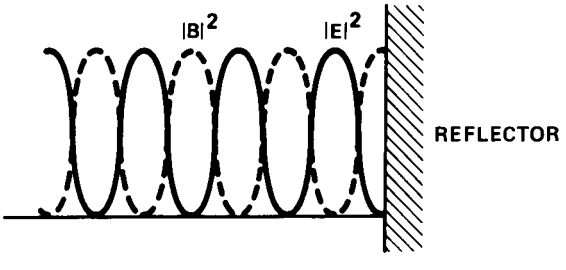

Fig. 1. Standing wave pattern of a reflected light wave in a vacuum.

inhomogeneous plasma, one would get the usual Airy-function pattern[4] of Fig. 2. As is well known, there is now a ponderomotive force,

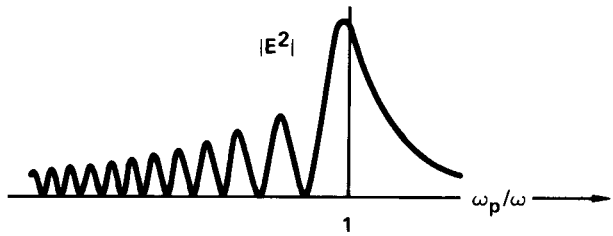

Fig. 2. Standing wave pattern of a light wave traveling along a plasma density gradient.

which reverses sign in each striation. This is because the oscillation of the plasma electrons causes $\underline{E}$ and $\underline{B}$ to have different amplitudes, so that $\nabla\langle E^2\rangle/8\pi$ and $\nabla\langle B^2\rangle/8\pi$ no longer cancel. The difference is proportional to the density. Since $ck/\omega = \varepsilon^{1/2}$ in a dielectric, Eq. (3) yields $\langle B^2\rangle = -\varepsilon\langle E^2\rangle$. Inserting this in Eq. (11), one has

$$\underline{F}_{NL} = (\varepsilon-1)\nabla\frac{\langle E^2\rangle}{8\pi} = -\frac{\omega_p^2}{\omega_0^2}\nabla\frac{\langle E^2\rangle}{8\pi} \quad , \tag{12}$$

as before. The macroscopic approach is so circuitous and opaque that derivations based on the Maxwell stress tensor are often erroneous.

ELECTROSTATIC PARAMETRIC INSTABILITIES

The parametric decay of an electromagnetic wave with $\omega_0 \simeq \omega_p$ into electrostatic perturbations has been extensively studied in recent years because of the applications to both ionospheric heating and laser-pellet heating. There are two processes, depending on the sign of $\omega_0-\omega_e$, where ω_e is the Bohm-Gross frequency, given by

$$\omega_e^2 = \omega_p^2 + 3k^2v_e^2 \quad . \tag{13}$$

For $\omega_0<\omega_e$, the oscillating two-stream (OTS) instability can occur, with $\mathrm{Re}\omega = 0$. For $\omega_0>\omega_e$, the parametric decay into an electron wave ω_e and an ion acoustic wave ω_i can occur. The reason for the difference is made clear by the ponderomotive force approach.

The Oscillating Two-Stream Instability

In the OTS instability, ω_0 is less than ω_e, and density ripples in the direction of $\underline{E}_0$ grow without propagating (Fig. 3). Let a

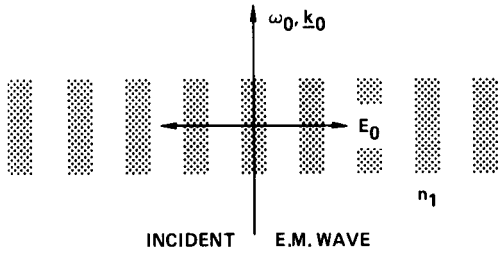

Fig. 3. Geometry of the OTS instability.

quasineutral density perturbation n_1 have $k >> k_0$, so that k_0 can be assumed to be zero and $\underline{E}_0$ to be uniform. The motion of electrons in the direction of $-\underline{E}_0$ will give rise to a space charge oscillating at the frequency ω_0, as shown in Fig. 4 at an instant when $\underline{E}_0$ is in the +x direction. This space charge creates a field $\underline{E}_1$

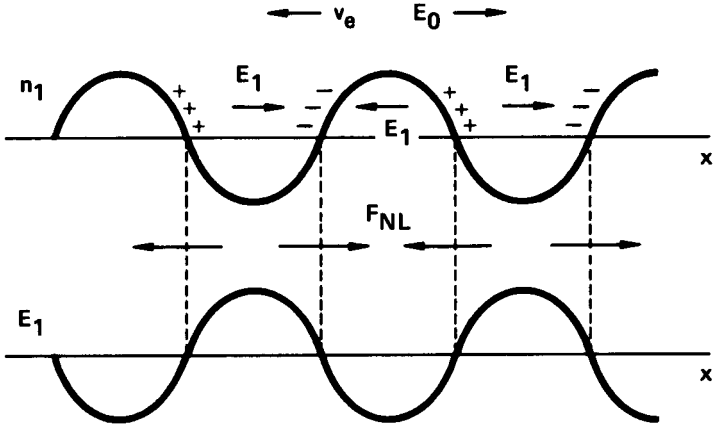

Fig. 4. Physical mechanism of the OTS instability.

with the phase shown in Fig. 4. For uniform $\underline{E}_0$, the ponderomotive force is given by

$$8\pi(\omega^2/\omega_p^2)\underline{F}_{NL} = -\nabla(\underline{E}_0+\underline{E}_1)^2 \simeq -2E_0\cdot\nabla E_1 = -2E_0\partial\underline{E}_1/\partial x \quad , \qquad (14)$$

and hence has the phase shown in the figure. Since the phase of $\underline{F}_{NL}$ is such as to move plasma into the regions of positive n_1, the density perturbation grows. Although these phase relationships hold for any $\omega_0<\omega_e$, excitation is easiest when ω_0 is near the

natural oscillation frequency ω_e of the electron fluid. The electrons move in a standing wave, but the ion motion does not follow a natural mode of the ion fluid. By symmetry, the ion perturbation does not propagate in either direction, and this is an absolute instability with $\mathrm{Re}\omega = 0$. It is possible[5] to recover from this ponderomotive force treatment the exact threshold and growth rates obtained by standard techniques[6]. A well-known theoretical result[6] is that the threshold for this instability depends on the damping rate γ_e of the electron waves, but not on the damping rate γ_i of ion waves. This is because the ions do not oscillate and suffer friction against another fluid but simply move slowly at the growth rate γ. By contrast, the electrons oscillate rapidly, and their motion is damped by collisions with ions and neutrals. Note that the $\underline{E}\times\underline{\nabla}\times\underline{E}$ part of F_{NL} does not enter in this geometry, since it gives a drift along planes of constant density.

The Parametric Decay Instability

If ω_0 is larger than ω_e, the OTS mechanism does not work; instead, the incident wave decays into an electron wave ω_e and an ion acoustic wave $\omega_i = kc_s$. Consider an oscillator x with natural frequency ω_e driven by a force $F\cos\omega_0 t$:

$$\ddot{x} + \omega_e^2 x = F\cos\omega_0 t\ , \qquad x = \frac{F\cos\omega_0 t}{\omega_e^2 - \omega_0^2}\ . \tag{15}$$

If $\omega_0 < \omega_e$, the displacement is in the same direction as the force, and the mechanism of Fig. 4 obtains. If $\omega_0 > \omega_e$, the displacement has the opposite sign, and electrons would move in the $+\underline{E}_0$ direction. As Fig. 5 shows, the resulting F_{NL} then acts so as to destroy a density perturbation n_1, which would then decay rather than grow. However, if the density ripple of wavenumber k were an ion wave traveling with velocity c_s, the phase relation can be reversed. In a frame moving with the ion wave, the density perturbation would be at rest, as in the OTS case. In the limit $k\lambda_D \ll 1$, the plasma is quasineutral, and the electron fluid follows the motion of the ion fluid very closely. However, in the

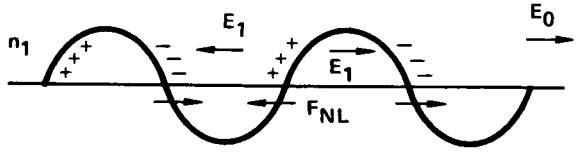

Fig. 5. Phase of F_{NL} relative to n_1 if $\omega_0 > \omega_e$.

moving frame the electron fluid feels the pump field $\underline{E}_0$ not at the frequency ω_0, but at the Doppler-shifted frequency $\omega_0' = \omega_0 - kc_s$. If $\omega_i = kc_s$ is sufficiently large, so that $\omega_0' < \omega_e$, the mechanism of the OTS instability can again operate, and the ion wave grows. Note that the critical condition $\omega_0 - kc_s = \omega_e$ is just the frequency-matching relation $\omega_0 = \omega_e + \omega_i$ for the decay process. Fig. 6A shows the usual parallelogram construction for ω and k matching in the parametric decay instability.

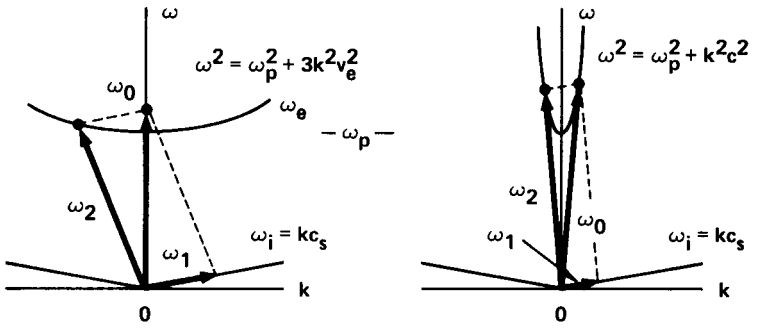

(A) DECAY INSTABILITY (B) BACKSCATTERING INSTABILITY

Fig. 6. Comparison of the ω and k matching conditions for electrostatic and electromagnetic parametric instabilities. In each case, ω_0 is the incident electromagnetic wave, and it decays into an ion wave ω_1 and another wave ω_2. In (A), ω_2 is an electron Bohm-Gross wave. In (B), ω_2 is a backscattered electromagnetic wave (Brillouin scattering). In Raman scattering, the ion wave is replaced by a Bohm-Gross wave.

BACKSCATTERING INSTABILITIES

Fig. 5B shows that backscattering is a parametric decay with one of the products being an electromagnetic wave. Since both ω_0 and ω_2 can be much larger than ω_p, backscattering can occur in an underdense plasma. For simplicity, we shall assume $\omega_0 >> \omega_p$ in describing the physical mechanism. Let ω_1 be electrostatic and ω_2 electromagnetic. The Stokes and anti-Stokes lines are given by $\omega_2 = \omega_0 \pm \omega_1$. In backscattering, the Stokes process (minus sign) is important, and the matching conditions are $\omega_0 = \omega_1 + \omega_2$, $\underline{k}_0 = \underline{k}_1 + \underline{k}_2$. The most likely process is for $\underline{k}_2$ to be opposite to $\underline{k}_0$, as shown in Fig. 7. Since $|k_2| \simeq |k_0|$ for $\omega_0 >> \omega_p$, we have $\underline{k}_2 \simeq -\underline{k}_0$ and, therefore, $\underline{k}_1 \simeq 2\underline{k}_0$.

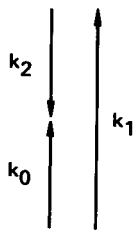

Fig. 7.

Let the incident wave be

$$\underline{E}_0 = E_0\hat{x}\cos(\omega_0 t - k_0 y).$$

The quiver velocity

$$\underline{v}_0 = -\frac{eE_0}{m\omega_0}\sin(\omega_0 t - k_0 y)\hat{x} \qquad (16)$$

then leads $\underline{E}_0$ by 90°. We look for a ponderomotive force $\underline{F}_{NL}$ at the relatively low frequency ω_1 of the electrostatic wave; this frequency results from the beating of the incident wave ω_0 with the backscattered wave ω_2. The relevant cross terms in Eq. (8) then give

$$\underline{F}_{NL} = -\frac{n_0 e^2}{m\omega_0^2}\langle \underline{E}_0 \cdot \nabla \underline{E}_2 + \underline{E}_2 \cdot \nabla \underline{E}_1 \rangle - \frac{en_0}{c}\langle \underline{v}_0 \times \underline{B}_2 + \underline{v}_2 \times \underline{B}_0 \rangle . \qquad (17)$$

The $\underline{E}\cdot\nabla\underline{E}$ terms vanish by geometry in straight backscattering, and $\underline{F}_{NL}$ is due entirely to the $\underline{v}\times\underline{B}$ terms. In Fig. 8A the two electromagnetic waves are shown at an instant of time when the maxima of

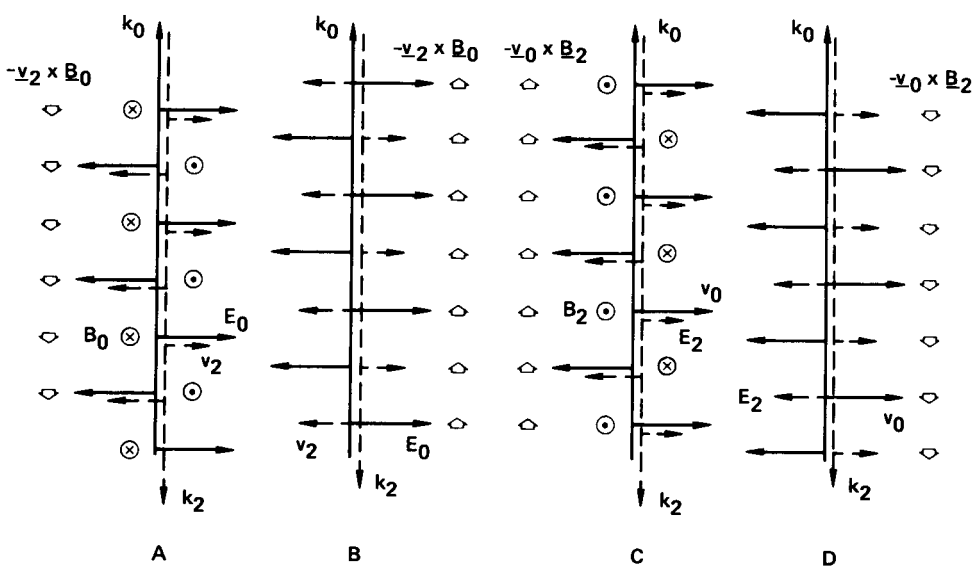

Fig. 8. Phase relationships in backscattering. The incident wave is indicated by solid lines; the backscattered wave by dashed lines. They heavy arrows indicate the ponderomotive force.

$\underline{E}_0$ and the quiver velocity $\underline{v}_2$ of the scattered wave are coincident. Taking $\underline{B}_0$ to be in the direction of $\underline{k}_0 \times \underline{E}_0$, one finds that the part of $\underline{F}_{NL}$ due to $-\underline{v}_2 \times \underline{B}_0$ is downward. As the waves pass, this term oscillates between 0 and its maximum value and hence has a finite average (over the ω_0 time scale) which depends on position. Fig. 8B shows the situation 1/4 of a period later. $\underline{E}_0$ has shifted upward and $\underline{v}_2$ downward; hence, $-\underline{v}_2 \times \underline{B}_0$ is upward at the locations shown. Making use of the fact that $\underline{v}$ leads $\underline{E}$ by 90°, one obtains Figs. 8C and 8D for the phases of the $-\underline{v}_0 \times \underline{B}_2$ term at the times corresponding to Figs. 8A and 8B, respectively, It is seen that the two terms in F_{NL} add in phase in such a way as to cause electrons to bunch up and form a density ripple with half the wavelength of the electromagnetic waves ($k_1 = 2k_0$). Thus, a density perturbation n_1 results from the nonlinear interference of the incident and backscattered waves, as depicted in Fig. 9.

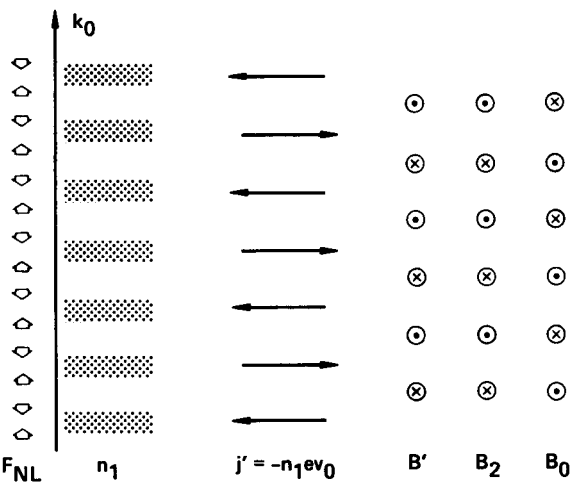

Fig. 9. Physical mechanism of backscattering instabilities.

It remains to show that n_1 causes the wave ω_2 to grow at the expense of the wave ω_0, closing the feedback loop for the instability. Since $\underline{v}_0$ is perpendicular to ∇n_1, we do not have the charge separation mechanism of the OTS instability. Instead, the effect is a spatial modulation of the oscillating current $-nev_0$ caused by $\underline{v}_0$. Let us neglect the motion of the density ripples and consider a phase 1/8 of a period after that of Fig. 8C. The

maxima of $\underline{v}_0$ and n_1 are then aligned, and the current modulation $\underline{j}' = -n_1 e \underline{v}_0$ is as shown in Fig. 9. This current generates a magnetic field $\underline{B}'$ with the phase shown. At this instant of time, examination of Fig. 8 shows that the phases of $\underline{B}_2$ and $\underline{B}_0$ are as given in Fig. 9. It is seen that $\underline{B}'$ is in phase with $\underline{B}_2$ and out of phase with $\underline{B}_0$, as needed for excitation of $\underline{B}_2$. The ponderomotive force approach can be used[7] to derive the exact results for these instabilities.

The density perturbation, as yet unspecified, may or may not be a natural mode of the plasma. We distinguish several cases:

1) If $\omega_1 = \omega_e$ (an electron plasma wave), the process is called stimulated Raman scattering (SRS).

2) If $\omega_1 = kc_s$ (an ion acoustic wave), the process is called stimulated Brillouin scattering (SBS).

3) If ω_1 is not a normal mode, the density perturbation can still exist if E_0 is large enough to maintain it against diffusion. This has been called resistive quasimode scattering.

4) If $\omega_1 = k_1 v_e$ or $k_1 v_i$, where v_e and v_i are thermal velocities, there can be interaction with resonant particles to give instability. This has been called induced Compton scattering or nonlinear Landau growth, a process that can be important when the natural modes are inhibited, say, by Landau damping.

Homogeneous Plasmas

The thresholds and growth rates for SBS and SRS in a homogeneous plasma have been computed by a number of authors[7-11] and are listed here for future reference. Note that v_0 is the peak quiver velocity in a plane-polarized wave. Here $v_e^2 = KT_e/m$, γ_i and γ_e are the ion and electron wave damping rates, and $(\omega_p^2/\omega_0^2)(\nu_{ei}/2)$ is the damping rate of the electromagnetic waves. The growth rates are for the intermediate-intensity regime (see below), where $\gamma_0 \propto E_0$. Note that γ_0 depends very weakly on density -- hence the possibility of anomalous reflection from the outer layers of a plasma. The collisional thresholds above are easily exceeded but are not relevant to actual experiments.

	Threshold	Growth Rate	
SBS	$\frac{v_0^2}{v_e^2} = \frac{8\gamma_i \nu_{ei}}{\omega_i \omega_0}$	$\gamma_0 \simeq \frac{1}{2}\frac{v_0}{c}(\omega_0/\omega_i)^{1/2}\omega_{pi}$	(18)
SRS	$\frac{v_0^2}{c^2} = \frac{2\omega_p^2}{\omega_0^2}\frac{\gamma_e}{\omega_p}\frac{\nu_{ei}}{\omega_0}$	$\gamma_0 \simeq \frac{1}{2}\frac{v_0}{c}(\omega_0\omega_p)^{1/2}$	(19)

Finite Homogeneous Plasmas

If the interaction region is limited in size either by the length of the plasma or the depth of focus of the laser beam, it is not sufficient to exceed the threshold; the growth rate must be large enough to overcome convection of wave energy out of the region. This problem has been treated by Pesme et al.[11], whose results may be summarized as follows. If ℓ is the length of the interaction region, γ_0 is the homogeneous-plasma growth rate given above, and V_1 and V_2 are the group velocities of the product waves, an absolute instability is possible if $V_1V_2 < 0$ and

$$\frac{\gamma_0\ell}{|V_1V_2|^{1/2}} > \frac{\pi}{2} \quad \text{or} \quad \frac{\gamma_0\ell}{(cc_s)^{1/2}} > \frac{\pi}{2} \quad \text{for SBS} \quad . \tag{20}$$

This result holds for weak damping such that $\gamma_0 >> \gamma_T$, where

$$\gamma_T \equiv (\gamma_1\gamma_2)^{1/2} = (\gamma_i\gamma_{ei}/2)^{1/2}(\omega_p/\omega_0) \quad \text{for SBS} \quad . \tag{21}$$

γ_T is just the threshold given in Eqs. (18) and (19).
We shall discuss specifically the Brillouin case, which has a higher nonlinear saturation level than Raman scattering. In SBS, ion Landau damping for reasonable ratios T_e/T_i causes γ_i/ω_i to be non-negligible. In such a case, the growth length is greatly increased by the damping, and Eq. (20) is valid only if γ_0 further satisfies $\gamma_0 >> \gamma_c$, where

$$\gamma_c \equiv \frac{1}{2}|V_1V_2|^{1/2}\left|\frac{\Gamma_1}{V_1} - \frac{\Gamma_2}{V_2}\right| \simeq \frac{1}{2}\gamma_i(c/c_s)^{1/2} \quad . \tag{22}$$

In most cases γ_0 lies in the range $\gamma_T < \gamma_0 < \gamma_c$, when no absolute instability is possible, but the waves can grow in space regardless of the sign of V_1V_2. The condition for a large number of e-foldings in ℓ is

$$\gamma_0{}^2\ell/c\gamma_i >> 1 \quad . \tag{23}$$

This condition is considerably more stringent than Eq. (20) and greatly reduces the large disparity between the SRS and SBS thresholds given in Eqs. (18) and (19).

These results can be understood physically as follows. In

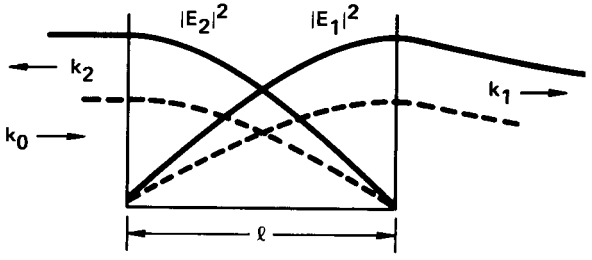

Fig. 10. Spatial variation of wave intensities in backscattering in a finite interaction region.

Fig. 10, we have shown schematically the behavior of the wave intensities in the weak-damping case (absolute instability). The pump wave is from the left; the ion wave grows from thermal noise from the left; and the backscattered wave grows from essentially zero amplitude from the right. To avoid questions of reflection from plasma boundaries, we assume the interaction region is limited by the focal depth alone, and the waves propagate with weak damping outside the region. The growth of each wave depends on the amplitude of the other one when it exits from the region. The light wave e-folds $\gamma_0\ell/c$ times in the length ℓ, while the ion wave e-folds $\gamma_0\ell/c_s$ times, c and c_s being the respective group velocities. Since each wave bootstraps the other, the net e-folding of the normal mode is the product of these two:

$$\frac{\gamma_0\ell}{c}\cdot\frac{\gamma_0\ell}{c_s} = \frac{\gamma_0^2\ell^2}{cc_s} > 1 \quad . \tag{24}$$

This is essentially Eq. (20). Thus it is the geometric mean of the group velocities which determines the convection.

In the intermediate damping case, γ_e [Eq. (22)] is determined by the ion wave damping, the light wave damping term being negligible. The damping length is c_s/γ_i. The growth length is $(cc_s)^{1/2}/\gamma_0$, since we have seen that $(cc_s)^{1/2}$ is the effective group velocity of the normal mode. For the damping length to exceed the growth length, we require

$$\frac{c_s}{\gamma_i} > \frac{(cc_s)^{1/2}}{\gamma_0} \quad , \quad \gamma_0 > \gamma_i(c/c_s)^{1/2} = 2\gamma_c \tag{25}$$

This is the meaning of γ_c. If $\gamma_0 < \gamma_c$, the ion wave loses energy

by damping more rapidly than by convection out of the growth region. In the length ℓ, the ion wave exponentiates $\gamma_0\ell/c_s$ times while being damped $\gamma_i\ell/c_s$ times. The net exponentiation is then γ_0/γ_i. Meanwhile, the light wave e-folds $\gamma_0\ell/c$ times. The product of the two is

$$\frac{\gamma_0}{\gamma_i} \cdot \frac{\gamma_0 \ell}{c} = \frac{\gamma_0^2 \ell}{c\gamma_i} \quad . \tag{26}$$

Eq. (23) is just the condition that this be >>1.

Inhomogeneous Plasmas

If the plasma is infinite but inhomogeneous, a different effect occurs. The plasma wave has a different wavelength in each part of the plasma, so that the matching conditions $\omega_0 = \omega_1+\omega_2$, $\underline{k}_0 = \underline{k}_1+\underline{k}_2$ can be satisfied only over a finite region. As a wave travels away from the point of perfect matching, it grows until the phase mismatch is so large that the proper phasing for growth is lost. The wave equation has a turning point there, and the wave propagates without growth from there on. The number of e-foldings is given by Eq. (24), with ℓ replaced by the distance ℓ_t between turning points. A turning point occurs when the phase mismatch $\int \Delta k dx \simeq \Delta k \ell_t$ is of order 1, where $\Delta k \simeq k'\ell_t$, $k' \equiv dk/dx$. Thus $\ell_t^2 \simeq 1/k'$, and Eq. (24) gives the approximate condition $\gamma_0^2/cc_s k' >> 1$ for appreciable growth. The exact number of e-foldings in E_2 is[12]

$$\pi\gamma_0^2/cc_s k' >> 1 \quad . \tag{27}$$

In SRS, k' is determined by the density gradient length L_n, since the Bohm-Gross dispersion relation depends sensitively on ω_p. In SBS, it is the temperature gradient length L_T which is important in the ion wave dispersion relation. Using these relations and the values of γ_0 from Eqs. (18) and (19), one obtains the following "inhomogeneous thresholds" from Eq. (27):

SBS
$$\frac{v_0^2}{v_e^2} > \frac{\omega_0^2}{\omega_p^2} \frac{8}{k_0 L_T} \tag{28}$$

SRS
$$\frac{v_0^2}{c^2} > \frac{2}{k_0 L_n} \quad . \tag{29}$$

Note that there is no density dependence in Eq. (29). This is because the density dependences in γ_0 and k' exactly cancel. Thus,

SRS can occur in a very underdense plasma. On the other hand, both Eq. (23) and Eq. (28) for SBS show that the threshold power varies as n_0^{-1} (when Landau damping dominates).

Nonlinear Behavior

Analysis of the nonlinear regime[9] shows that the growth rate (both temporal and spatial) varies with pump amplitude in the manner shown in Fig. 11. Region B is the region of linear growth rate described by Eqs. (18) and (19). Since the electrostatic

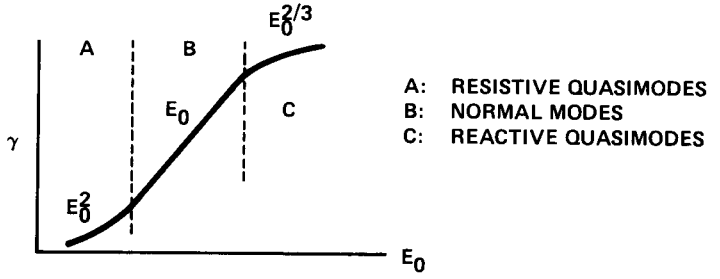

Fig. 11. Behavior of the growth rate of parametric instabilities with pump amplitude.

wave, say ω_i, is driven by the ponderomotive force, the ion wave equation is of the form

$$\omega^2 - \omega_i^2 + 2i\gamma_i\omega \propto F_{NL} \propto E_0^2 \quad . \tag{30}$$

In region B, the damping term is negligible, and the quadratic equation yields $\gamma \propto E_0$. In region A, only broad, damped responses rather than normal modes are excited. In this case, $2i\gamma_i\omega$ term dominates in Eq. (30), and γ is proportional to E_0^2. In region C, the ponderomotive force is so strong that the right-hand side of Eq. (30) determines the frequency ω rather than the natural frequency ω_i. The $E_0^{2/3}$ dependence of γ is a result of optimizing the phase shift $\omega-\omega_i$, a process for which we have not found a simple physical explanation. The result is that a factor ω appears in the denominator of the right-hand side of Eq. (30), making the equation a cubic in ω, so that $\gamma \propto E_0^{2/3}$. This behavior at large amplitudes is quite general[6].

Nonlinear saturation levels in collisionless plasmas with $\omega_0 \simeq 10\omega_p$ have been investigated by numerical simulations in one dimension[9,13]. Although SRS grows faster than SBS, the former is easily saturated so that no more than 50% of the incident energy

is reflected. Possible saturation mechanisms for SRS are electron trapping, electron heating followed by increased Landau damping, mode-coupling followed by nonlinear Landau damping, and modulational instabilities. The last mechanism[8] is the refraction of plasma waves away from regions of high density because the index of refraction for them is less than unity. The waves then pile up in regions of low density, and the ponderomotive force causes the density to decrease further there. The large resulting density perturbations stabilize the backscattering by the inhomogeneity effect. Ion waves are not subject to these saturation mechanisms, and consequently SBS is expected to grow to large amplitudes. In numerical simulations, there are relaxation oscillations with reflected power reaching 99%. Given enough time, however, the light pressure eventually causes the incident wave to bore through any finite thickness of plasma in spite of SBS instabilities. At the point where $\omega_0 = 2\omega_p$, a particularly strong interaction occurs which causes a rift in the plasma. This has a simple physical explanation: SRS occurring at this point generates a scattered wave $\omega_2 = \omega_p$. This wave cannot propagate out of the plasma and is trapped.

SIDESCATTERING

Consider now the orientation of wave vectors as the angle θ between $\underline{k}_1$ and $\underline{k}_0$ is changed, as in Fig. 12. Since $|k_0|$ and $|k_2|$ are fixed at $\simeq \omega_0/c$ for $\omega_0 >> \omega_p$, the locus of the tip of the $\underline{k}_1$ vector lies on a circle. It is clear from the geometry that $\underline{k}_0$ and $-\underline{k}_2$ are at an angle 2θ.

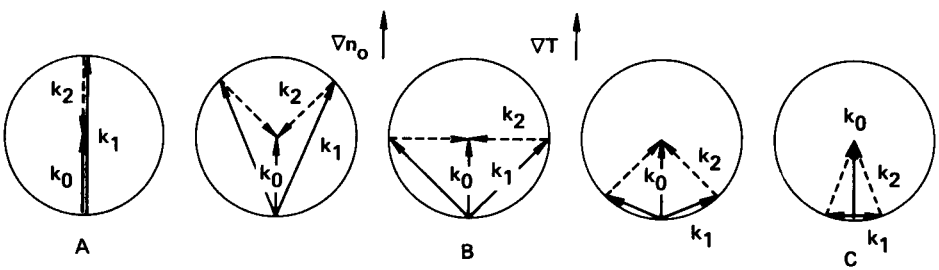

Fig. 12. Vector relations for (A) backscattering, (B) sidescattering, and (C) forward scattering. The incident, electrostatic, and scattered electromagnetic waves are $\underline{k}_0$, $\underline{k}_1$, and $\underline{k}_2$ respectively; and $\underline{k}_0 = \underline{k}_1 + \underline{k}_2$.

Case A in Fig. 12 is backscattering. Case C is forward scattering; this is a weak interaction because $\underline{k}_1$, and hence the electrostatic field, is small. Case B, sidescattering, is important if $\underline{k}_0$ is parallel to the plasma gradients. The wave $\underline{k}_2$ then propagates at right angles to the gradients and does not suffer the

phase mismatch due to plasma inhomogeneity. For SRS, Mostrom et al.[14] find that the growth rate in an inhomogeneous plasma is limited only by the beam radius $\underline{a}$ (cm) and the damping rate γ_e. They have also calculated statistically the required number G of e-foldings from the thermal level. For CO_2, the threshold intensities are:

$$\text{Sidescattering:} \quad I_s > 4.5\, G_s\, \gamma_l/\omega_p a \times 10^{12}\ \text{W/cm}^2 \tag{31}$$

$$\text{Backscattering:} \quad I_b > 0.7\, G_b/L_n \times 10^{12}\ \text{W/cm}^2 \tag{32}$$

where $G_s \simeq 35$ and $G_b \simeq 30$. Eq. (32) agrees with Eq. (29) for $G_b = 2\pi$. Thus, depending on the ratio a/L_n, sidescattering may be as important as backscattering if the plasma is inhomogeneous.

The physical mechanism of sidescattering is illustrated in Fig. 13.

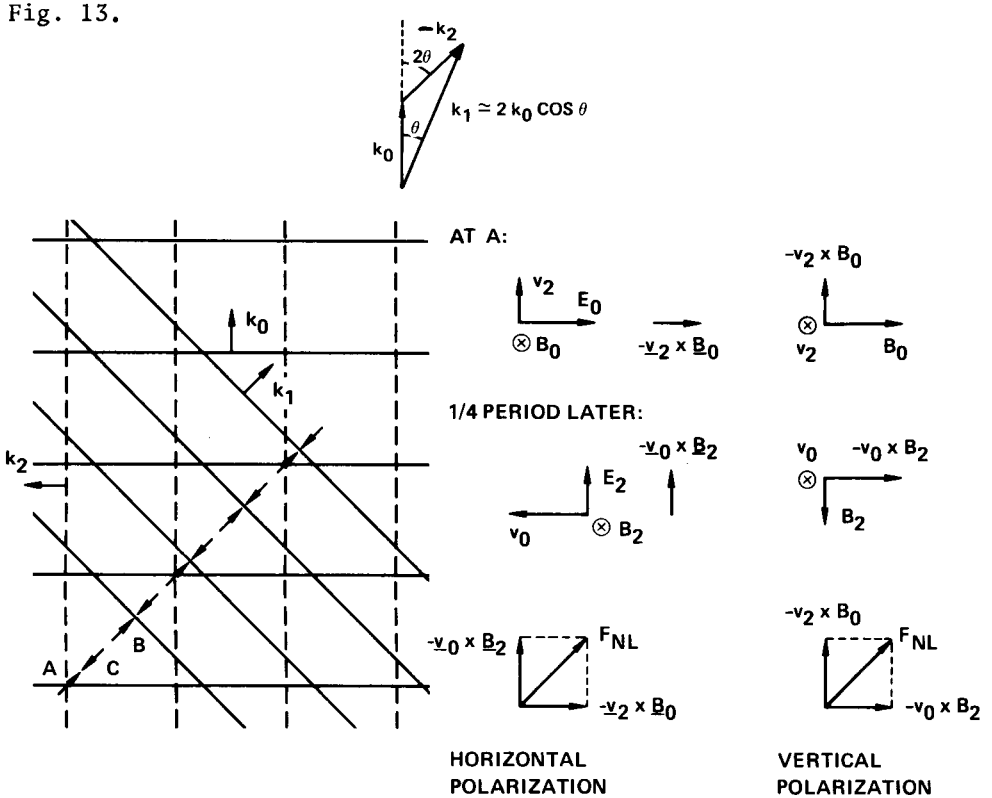

Fig. 13. Physical mechanism of sidescattering.

The wave fronts of the incident wave $\underline{k}_0$, traveling upward, are shown by the solid lines. The dashed lines show the wave fronts of the sidescattered wave $\underline{k}_2$, traveling to the left. For the case

of horizontal polarization, $\underline{E}$ is in the plane of the page, and the wave $\underline{k}_2$ is simply rotated by 90° from Fig. 8. At the point A, $\underline{E}_0$ and $\underline{v}_2$ are assumed to be at their maxima. As shown in the center column of Fig. 13, the term $-\underline{v}_2 \times \underline{B}_0$ of the ponderomotive force $\underline{F}_{NL}$, Eq. (17), is then to the right. At the same point A a quarter period later, $\underline{v}_0$ and $\underline{B}_2$ are in phase, and the term $-\underline{v}_0 \times \underline{B}_2$ is upward. Since these two terms are equal in magnitude, the resultant $\underline{F}_{NL}$ is at 45°, as shown. At the point B in Fig. 13, both $\underline{v}$ and $\underline{E}$ are reversed in direction, and $\underline{F}_{NL}$ is the same as at A. At the point C, $\underline{v}$ and $\underline{E}$ are shifted 90° from A in opposite directions; their product, therefore, is the negative of that at A, and $\underline{F}_{NL}$ is in the opposite direction. The resulting pattern of the ponderomotive force causes density striations at $\theta = 45°$, in agreement with Fig. 12B. The wavelength is $\lambda_0/2 \cos\theta$, or $k_1 = 2k_0 \cos\theta$--also in agreement with the geometrical construction of Fig. 12.

This polarization is not the optimum for excitation, however, because of the $\underline{E}\cdot\nabla\underline{E}$ terms in Eq. (17), which we have neglected. These terms oppose the $\underline{v} \times \underline{B}$ terms in the $\theta = 45°$ case and diminish the net $\underline{F}_{NL}$. The $\underline{E}\cdot\nabla\underline{E}$ terms identically vanish by geometry in the case of vertical polarization, in which both $\underline{E}_0$ and $\underline{E}_2$ are out of the page. In that case, $\underline{B}_0 - \underline{B}_2$ are in the plane of the page, and the vectors in the third column of Fig. 13 indicate the total ponderomotive force.

Note that the regular spacing of the density ripples in Fig. 13 is possible in SRS only if $T_e = 0$, so that $\omega = \omega_p$. For finite T_e, the Bohm-Gross dispersion relation requires k_1 to vary with ω_p. The wave fronts of $\underline{k}_1$ must then be curved, and a plane wave $\underline{k}_2$ cannot exist without phase mismatches even in sidescattering.

We wish now to explain the angular dependence of stimulated Brillouin scattering, whose growth rate[7] varies as $\cos\phi(\cos\theta)^{\frac{1}{2}}$ where ϕ is the polarization angle between $\underline{E}_0$ and $\underline{E}_2$. The $\cos\phi$ factor is easily understood, since the entire expression of Eq. (17) for $\underline{F}_{NL}$ is proportional to $\nabla \langle \underline{E}_0 \cdot \underline{E}_2 \rangle$. The $\cos\theta$ factor is best seen from the $\underline{v} \times \underline{B}$ terms in the case $\phi = 0$, when the $\underline{E}\cdot\nabla\underline{E}$ terms vanish. From Eq. (9) it is clear that $\underline{F}_{NL}$ is proportional to $\langle \underline{E}_0 \times (\underline{k}_2 \times \underline{E}_2) \rangle + \langle \underline{E}_2 \times (\underline{k}_0 \times \underline{E}_0) \rangle$. These terms are of equal magnitude and are in the directions of $\underline{k}_2$ and $\underline{k}_0$, respectively. The phases are such that the averages are of opposite sign. The total F_{NL} is, therefore, proportional to $|\underline{k}_0 - \underline{k}_2|$. From Fig. 12, we see that $|\underline{k}_0 - \underline{k}_2| = |k_1| \simeq 2k_0 \cos\theta$. The growth rate γ_0 is proportional to F_{NL}, and hence to $\cos\theta$. In Eq. (18), however, we see that γ_0 is also proportional to $\omega_i^{-\frac{1}{2}} = (k_1 c_s)^{-\frac{1}{2}} \simeq (2k_0 c_s \cos\theta)^{-\frac{1}{2}}$. This additional factor is due to the fact that the electric field in the ion wave depends on its wavelength. The growth rate γ_0, therefore, varies as $(\cos\theta)^{\frac{1}{2}}$. This weak dependence on θ, which is valid only for linear ion waves, is in disagreement with the experimental observations of Eidmann and Sigel[15], which show strongly collimated

backscattering. If the ion waves are nonlinear, however, it is possible that the fastest growing mode--that with $\theta=0$--is the only one that survives.

FILAMENTATION

Filamentation, or self-focussing, occurs when the incident wave vector lies along incipient density striations (Fig. 14). The refraction caused by the density perturbations of wave number k_1 channels the light beam into the less dense regions. The resulting ponderomotive force pushes plasma away from such regions and increases the density perturbations. In steady-state, F_{NL} balances the electron pressure $\nabla(nKT_e)$, giving rise to the Boltzmann-like relation

$$n = n_0 \exp - \left[\frac{\omega_{p0}^2}{\omega_0^2} \frac{\langle E^2 \rangle}{8\pi n_0 KT_e}\right] \tag{33}$$

which is independent of gradient scale length.

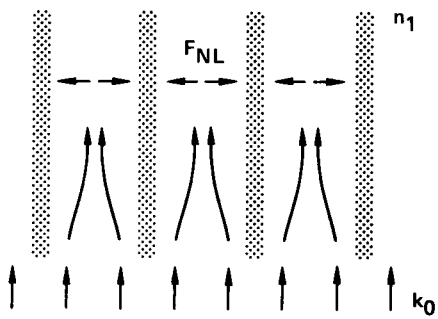

Fig. 14. Physical mechanism of filamentation.

If the light waves are not damped and Debye shielding were perfect, this equilibrium would occur with any intensity; and there would be no threshold for filamentation. The deviation from strict neutrality due to finite Debye length, however, means that F_{NL} must overcome a small electric field proportional to $k_1^2\lambda_D^2$. The filamentation threshold given by Kaw et al.[7,16] is

$$\frac{v_0^2}{c^2} > 4\left(1 + \frac{T_i}{T_e}\right)k_1^2\lambda_D^2 \tag{34}$$

The first density perturbations that grow will be of smallest k_1 and longest wavelength, comparable to the plasma or beam radius. Since v_0^2 is proportional to intensity, or power divided by beam radius, the threshold for self-focussing depends only on total

beam power. For a Gaussian beam, this threshold is

$$P_c = 8500(\omega_c/\omega_p)^2 T_{eV} \quad \text{watts} \quad . \tag{35}$$

For $k_1 \simeq r^{-1}$, Eqs. (34) and (35) are identical to within a numerical factor. Although the threshold for filamentation is lower than that for absolute parametric instabilities, the growth rate is slower [7,16]:

$$\gamma \simeq \frac{1}{2}\frac{v_0}{c}\omega_{pi} \quad . \tag{36}$$

This is a factor $(\omega_i/\omega_0)^{1/2}$ smaller than that given in Eq. (18) for SBS.

The preceding picture of self-focussing is well-known; indeed, it was the first application of the ponderomotive force. This phenomenon, however, can also be considered a parametric instability in which the ion wave $\underline{k}_1$ is at right angles to $\underline{k}_0$, as in Fig. 12C. Since $\underline{k}_1$ is small in this limit, the anti-Stokes process $\underline{k}_2 = \underline{k}_0 + \underline{k}_1$ is indistinguishable from the Stokes process $\underline{k}_2 = \underline{k}_0 - \underline{k}_1$; and both must be considered. Filamentation is, therefore, a four-wave, rather than a three-wave, interaction. [The anti-Stokes diagrams corresponding to Fig. 12 are obtained by reversing the directions of the $\underline{k}_1$ arrows.] The forward-scattered waves $\underline{k}_2$ interfere with the incident wave to produce the refraction and self-focussing in the usual physical picture. The geometry of this instability is identical with that of the OTS instability (Fig. 3), and both are non-convective. However, Since $\underline{k}_2$ is a light wave, the simplification $k_0 << k_1$ cannot be made in filamentation.

OPTICAL MIXING AND CASCADING

By using two lasers with a frequency difference, it is possible to couple strongly to an underdense plasma by making $\omega_0 - \omega_1 = \omega_p$. This was first suggested by Kroll, Ron, and Rostoker[17] and experimentally tested by Stansfield, Nodwell, and Meyer[18]. Recent work[19,20,21] treats nonlinear saturation and plasma inhomogeneity. Fig. 15 illustrates the basic idea. In the Raman process, two electromagnetic pump waves ω_0 and ω_2 beat with each other to

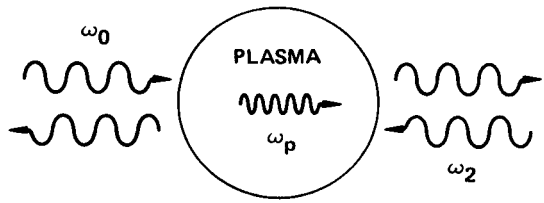

Fig. 15. Laser-beating at $\Delta\omega = \omega_p$.

generate a plasma wave ω_1, such that $\omega_0 - \omega_2 = \omega_1 \simeq \omega_p$, $\underline{k}_0 - \underline{k}_2 = \underline{k}_1 \simeq 2\underline{k}_0$. The plasma wave, in turn, interacts with the incident waves to change their amplitudes: the higher-frequency wave ω_0 is damped, while the lower-frequency wave ω_2 is enhanced. The interaction is strongest with $\underline{k}_2 = -\underline{k}_0$, as shown. This process will be recognized as just stimulated backscattering: the backscattered wave ω_2, with the proper frequency shift, is imposed on the plasma, so that it does not have to grow from thermal noise. The threshold, therefore, is lower than in SRS. The theory differs only in that the amplitude of ω_2 is assumed fixed, with the consequence that the ω_p oscillation grows linearly with time rather than exponentially.

It is tempting to try to heat a plasma by this anomalous absorption process. For instance, the 10.6μ and 10.2μ lines of the CO_2 laser can beat to couple with a plasma of density 1.5×10^{16} cm^{-3}, or the 10.6μ and 9.6μ lines with $n = 10^{17}$ cm^{-3}. Unfortunately, the energy given to the wave ω_1 is much less than the energy exchange between ω_0 and ω_2. This is a consequence of the conservation of action. From a quantum mechanical viewpoint, the energy of a wave is $W = N\hbar\omega$, where N is the number of quanta. Since N is conserved, one has

$$\frac{W_0}{\omega_0} = \frac{W_1}{\omega_1} = \frac{W_2}{\omega_2} \quad , \tag{37}$$

where W_1 is small because $\omega_1 << \omega_0, \omega_2$. However, the wave momenta $\underline{p} = N\hbar\underline{k}$ are such that they add rather than subtract, and electromagnetic momentum can be transferred to the plasma to achieve low-frequency coupling[22].

To circumvent the restriction on energy coupling, Kaufman et al.[23] suggested a cascade process (Fig. 16). Two incident beams

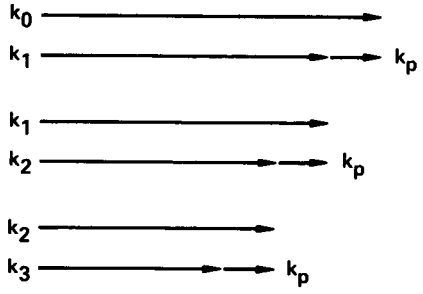

Fig. 16. Decay of wave vectors in cascading.

$\omega_0, \underline{k}_0$ and $\omega_1, \underline{k}_1$ undergo forward scattering to produce a plasma wave $\omega_p = \omega_0 - \omega_1$, $\underline{k}_p = \underline{k}_0 - \underline{k}_1$. The plasma wave then interacts with $\underline{k}_1$ to produce $\omega_2 = \omega_1 - \omega_p$, $\underline{k}_2 = \underline{k}_1 - \underline{k}_p$, and so forth until the laser energy is almost all converted into plasma waves. Repeated k-matching, unfortunately, works only for forward scattering, which is ω_p/ω_0 times less efficient than backscattering. Because of this, the threshold for cascading is rather high.

KINETIC INSTABILITIES

There are a number of parametric instabilities involving resonant particles which cannot be treated by fluid theory. One of these is nonlinear Landau growth, discussed previously. Another is a kinetic modulational instability, which is driven by particles resonant with the group velocity v_g of a large amplitude wave. The physical mechanism is made clear in Fig. 17. The ponderomotive

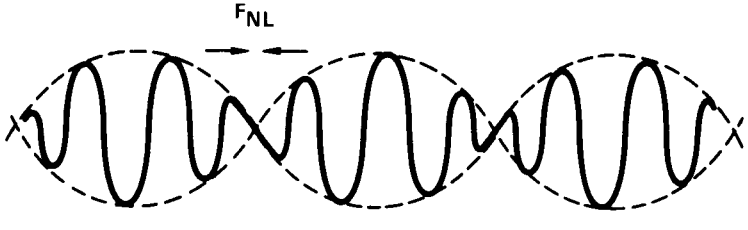

Fig. 17. Mechanism of kinetic modulational instabilities.

force associated with the envelope of a modulated wave interacts with particles traveling near v_g to produce Landau damping or growth, depending on the sign of $f_0'(v_g)$.

The plasma laser is an interesting idea suggested by J.M. Dawson. Let a density ripple of wavenumber k_i exist in a plasma, and let a light wave $\underline{E}_0$ with frequency ω_0 and $k_0 \ll k_i$ be imposed (Fig. 18). As in the OTS instability, a high-frequency field $\underline{E}_1$ is set up by charge separation. The field $\underline{E}_1$ is the sum of two waves with phase velocities $\pm\omega_0/k_i$ and can therefore interact with particles at these velocities. If the electron distribution is

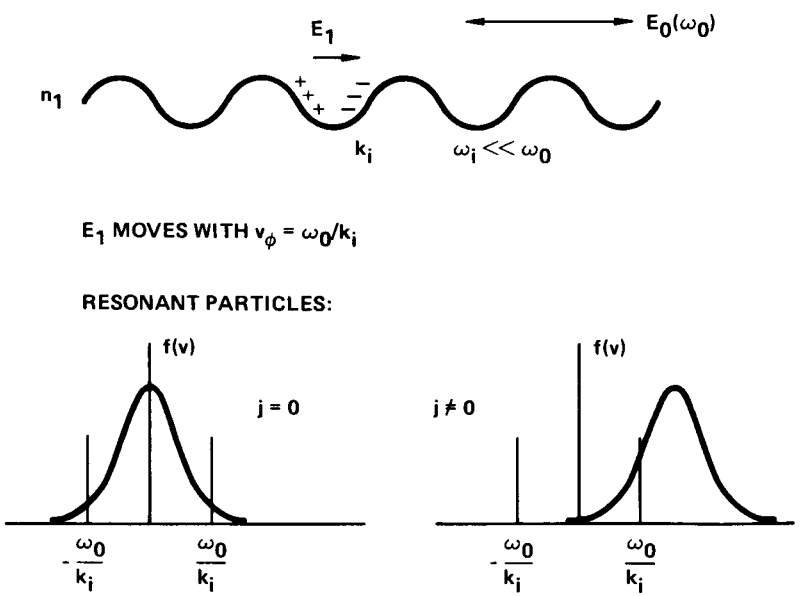

Fig. 18. Mechanism of the plasma laser.

symmetric, no instability occurs. However, if a current exists in the plasma, so that f(v) is shifted as in the lower right-hand part of Fig. 18, the resonant particles can feed energy into E_1, and hence E_0. Thus, lasing action occurs without molecular transitions.

The author is indebted to Prof. George Schmidt for a large number of clarifying discussions.

REFERENCES

1. H. Hora, Laser Interaction and Related Plasma Phenomena, ed. by H.J. Schwarz and H. Hora (Plenum Press, New York, 1971), p. 383 ff.
2. G. Schmidt, Physics of High Temperature Plasmas (Academic Press, New York, 1966), p. 47 ff.
3. J.W. Shearer and J.L. Eddleman, Lawrence Livermore Laboratory UCRL-73969 (1972).
4. V.L. Ginzburg, Propagation of Electromagnetic Waves in Plasmas (Pergamon Press, New York, 1964), p. 365.
5. A.Y. Wong and G. Schmidt, UCLA PPG-151 (1973).
6. K. Nishikawa, J. Phys. Soc. Japan 24, 916 (1968).
7. J. Drake, P.K. Kaw, Y.C. Lee, G. Schmidt, C.S. Liu, and M.N. Rosenbluth, UCLA PPG-158 (1973).
8. M.N. Rosenbluth and R.Z. Sagdeev, Comments on Plasma Physics and Controlled Fusion 1, 129 (1972).
9. D.W. Forslund, J.M. Kindel, and E.L. Lindman, to be published; also Phys. Rev. Lett. 30,739 (1973).
10. C.S. Liu and M.N. Rosenbluth, Inst. for Advanced Study COO 3237-11 (1973).
11. D. Pesme, G. Laval, and R. Pellat, Phys. Rev. Lett. 31, 203 (1973); also D. Pesme, Thesis, Univ. of Paris (1973).
12. M.N. Rosenbluth, Phys. Rev. Lett. 29, 565 (1972).
13. W. Kruer, Lawrence Livermore Laboratory, private communication.
14. M.A. Mostrom, D.R. Nicholson, and A.N. Kaufman, Lawrence Berkeley Laboratory LBL-2032 (1973).
15. K. Eidmann and R. Sigel, Inst. f. Plasmaphysik, Garching, Germany, IPP IV/46 (1972).
16. P.K. Kaw, G. Schmidt, and T. Wilcox, UCLA PPG-140 (1972).
17. N.M. Kroll, A. Ron, and N. Rostoker, Phys. Rev. Lett. 13, 83 (1964).
18. B.L. Stansfield, R. Nodwell, and J. Meyer, Phys. Rev. Lett. 26, 1219 (1971).
19. M.N. Rosenbluth and C.S. Liu, Phys. Rev. Lett. 29, 701 (1972).
20. G. Schmidt, UCLA PPG-133 (1972).
21. A.N. Kaufman and B.I. Cohen, Phys. Rev. Lett. 30, 1306 (1973).
22. F.F. Chen, Comments on Plasma Physics and Controlled Fusion 1, 81 (1972).
23. B.I. Cohen, A.N. Kaufman, and K.M. Watson, Phys. Rev. Lett. 29, 581 (1972).